

Influence of Incorporating MWCNTs on Some Physical Characteristics of Blend Nanocomposites

Lubna Abdul-Aziz Jassim^{1a} and Mohammed Kadhim Jawad^{1b*}

¹Department of Physics, College of Science, University of Baghdad, Baghdad, Iraq

^aE-mail: lubnaabdalaziz93@gmail.com

^{b*}Corresponding author: mohamedkadhom@sc.uobaghdad.edu

Abstract

Nanocomposite membranes made of chitosan (Cs) concentrations, and polyvinyl alcohol (PVA) with a fixed ratio of (60:40), then incorporated with different concentrations of multi-walled carbon nanotubes (MWCNTs) (1, 1.5, 2, 2.5, and 3%) were created using the solution cast method. The membranes were identified using UV-vis spectroscopy, Fourier transform infrared (FTIR), and X-ray diffraction (XRD). The results demonstrated that the samples were sufficiently stable, and the interactions between nanoparticles and polymers were generally negligible. XRD patterns showed a crystalline phase of PVA, an amorphous phase of chitosan, and a more crystalline phase as MWCNTs were introduced. In particular, at high percentages of MWCNTs, the dominant phase (002), connected to MWCNTs, was shifted to a higher value. The UV-vis spectroscopy of the sample showed only one absorption peak at about 230 nm and no other peaks. This may be due to transparency in PVA and Cs. The band gap energy decreased when higher percentages of MWCNTs were added to the mixture.

Article Info.

Keywords:

Chitosan, Polyvinyl Alcohol, Multi-Wall Carbon Nanotube, Nanocomposites, Morphological Properties.

Article history:

Received: Sep. 27, 2023

Revised: Dec. 18, 2023

Accepted: Dec. 29, 2023

Published: Mar. 01, 2024

1. Introduction

Because of environmental concerns, natural materials are again in vogue [1]. Biodegradable polymers and plastics are increasingly used in modern industrial and academic applications [2]. Recycling and environmental safety become crucial when considering a more sustainable future [3]. Interest in polymer composites with organic and natural fillers is rising due to the demand for more adaptable polymer-based products [4]. For instance, fillers can be recycled and decomposed [5]. Biomaterials are becoming increasingly important in creating a sustainable environment [6]. The creation of biomaterials for drug delivery, tissue engineering, and medical diagnostics is still relatively new, but physical and chemical techniques to control biological reactions have made significant advances [7]. The best definition of a biomaterial is any substance, other than drugs or synthetic materials, that can be used at any time to partially or entirely replace any tissue or other part of the body and improve an individual's quality of life [8]. Four different biomaterials, polymers, metals, ceramics, and composites are widely known in the industrial world [9].

Polysaccharide biopolymers are the second most frequent biopolymers of biological origin. Natural chitosan is an example of these biopolymers. It can be produced synthetically utilizing chitin as a raw material source by a deacetylase reaction and is derived from shrimp, crab molluscs, lobster shells, and prawns [10, 11]. Chitin is a natural polymer, a source of biodegradable polysaccharide polymer. It is renewable, non-toxic, and has an excellent chemical makeup. It also has high film-forming abilities and is soluble in slightly acidic aqueous solutions. It is an entirely biodegradable product that can be buried without interfering with the natural flow of the ecosystem. Chitosan is frequently used in wound healing and bandaging because of its exceptional qualities, including antibacterial activity, biocompatibility, and non-toxicity. Chitin's

drawbacks include susceptibility to degradation by ultraviolet radiation, difficulty in spinning leading to lack of wet strength, and low water solubility due to low thermal stability [12].

Polymer blending presents an intriguing way to produce novel polymeric materials with tailored qualities better suited to each polymer product. A polymer blend (PB) is created when two or more polymers or copolymers are combined and given particular physical qualities [13]. The synthetic polymer polyvinyl alcohol (PVA) has good chemical, physical, and mechanical qualities and is non-toxic and water-based [14]. PVA, a water-soluble polymer with remarkable mechanical qualities and great transparency, is utilized in a wide range of domestic, commercial, and electrical products. PVA is a polyhydroxy polymer frequently employed in advantageous applications due to its simplicity of manufacture and biodegradability [15]. Even though they can be used in tandem with other natural polymers and synthetic polymers combined with natural polymers, modified polymers can achieve the desired properties [16].

A significant area of study is nanocomposites [17], which are created by dispersing nanoparticles, such as metal nanoparticles or metal oxides, onto a polymer substrate. Nanotechnology has recently made scientific discoveries that have been used in manufacturing, agriculture, and medicine, among other fields [18]. Compared to micro and macro composites, nanoparticles have better mechanical and thermal properties and less flammability. The factors that play a significant role in modifying the properties of composites are their shape, proportion, and affinity toward the matrix [19].

Carbon nanotubes (CNTs) are single-layer graphene rolled into tubes [20]. Single-walled carbon nanotubes (SWCNTs) were found in 1991 by Iijima and Ichihashi [21]. They detailed the development of 1 nm SWCNT by carbon bend union. Like fullerene and graphene, SWCNT is one of the isotropic shapes of carbon [22]. The term settled SWCNT refers to multi-walled carbon nanotubes (MWCNTs), freely bound together by Van der Waals intuitive [23]. The bond between carbon gives carbon nanotubes not only uncommon flexibility quality but too great conductivity [24]. CNTs have many interesting properties, such as electrical conductivity, which have been investigated in many studies [25]. The diameter of CNT is usually measured in nanometers. It is one of the most widely used nanomaterials due to its wide variety of physicochemical properties, such as a field emitter, hydrogen storage medium, and sensor [26]. Techniques such as Fourier transform infrared (FTIR), and X-ray diffraction (XRD), which detect variations in chemical groups and chemically related states, have been used to quantify surface chemical changes in modified materials [27].

This study investigated the influence of MWCNTs weight ratio on the properties of PVA/chitosan nanocomposite membranes [10].

2. Experimental Work

The chemical materials used were: polyvinyl alcohol (PVA) (molecular weight 85,000, DH= 99.8%), chitosan medium molecular (75–85% deacetylate), chemical formula $(C_2H_4O)_n$, and MWCNTs with outer diameter 13-18 nm, length 3-30 nm and purity >99.0 %.

Polymers (chitosan, PVA) and their mixtures in a fixed ratio of (60: 40) and nanocomposite membranes were prepared using the solution casting process. The basic PVA solution was prepared by dissolving 0.6 g of PVA (at 80 °C) in 8 ml of distilled water. 0.4 g of chitosan was dissolved in 20 ml of acetic acid and heated to 50°C with continuous stirring for approximately 8 hours at 30°C. A polymer mixture of (PVA and Chitosan) with a fixed ratio of (60:40) was prepared by adding the chitosan solution to

PVA solution using a magnetic stirrer for 24 hrs. The solution was continuously stirred until a homogeneous aqueous solution was obtained. MWCNTs filled nanocomposites were prepared using the same curing procedure above. Polymer mixtures incorporating different percentages of MWCNTs (1, 1.5, 2, 2.5, and 3%), as tabulated in Table 1, were prepared. Finally, each mixture was poured into glass petri dishes and left to dry at room temperature to form solid membranes. After 72 hrs, the membranes were peeled off the plate.

Table 1: The composition of the blended and nanocomposite membranes.

Assignment	Name of the polymer	Weight percent %	Nano-MWCNT wt.%
Cs	Chitosan	100%	0
PVA	Polyvinyl alcohol	100%	0
Cs& PVA	Chitosan: Polyvinyl alcohol	40:60%	0
C1	Chitosan: Polyvinyl Alcohol	40:60%	1
C2	Chitosan: Polyvinyl Alcohol	40:60%	1.5
C3	Chitosan: Polyvinyl Alcohol	40:60%	2
C4	Chitosan: Polyvinyl Alcohol	40:60%	2.5
C5	Chitosan: Polyvinyl Alcohol	40:60%	3

3. Characterization of Chemical Structure Materials

The FTIR spectra were recorded from 4000 to 400 cm^{-1} , using the absorption mode with 32 scans and 2 cm^{-1} resolution for analysis, using a Nicolet beam line with 10 spectrometers. The optical properties of the sample were identified using a UV-vis spectrophotometer (V-570 UV/vis-NIR, JASCO Corp) running at room temperature. XRD patterns were recorded with a Shimadzu XRD 6000 diffractometer at the College of Education-Ibn Al Haitham. The XRD system uses a Cu (K) X-ray source (1.5405), 40 kV voltage, and 30.0 mA current. The scanning angle was changed at a rate of 5.00 (degrees/minute) along the range of ($2\theta = 5-80$).

4. Results and Discussion

4.1. FTIR Results

FTIR spectroscopy is an essential technique in observing the band structure of materials, which changes depending on the details, complexity, and interactions between different components such as polymers, net chitosan, and PVA [28]. Figure 1 shows the FTIR spectra of pure Cs, PVA, and Cs: PVA mixture. The characteristic peak of PVA was observed at 3501.25 cm^{-1} , related to the O-H relaxation vibration. Additional peaks at 2950 and 2908.75 cm^{-1} were observed due to the symmetric and asymmetric expansion vibrations of the CH_2 beam. The peak found at 1570.00 cm^{-1} was attributed to the impact of C-O knife edge expansion of amide ($-\text{NH}_2$). Bands type and energies for pure chitosan, PVA, and Cs: PVA mixture are listed in Table 2 [29].

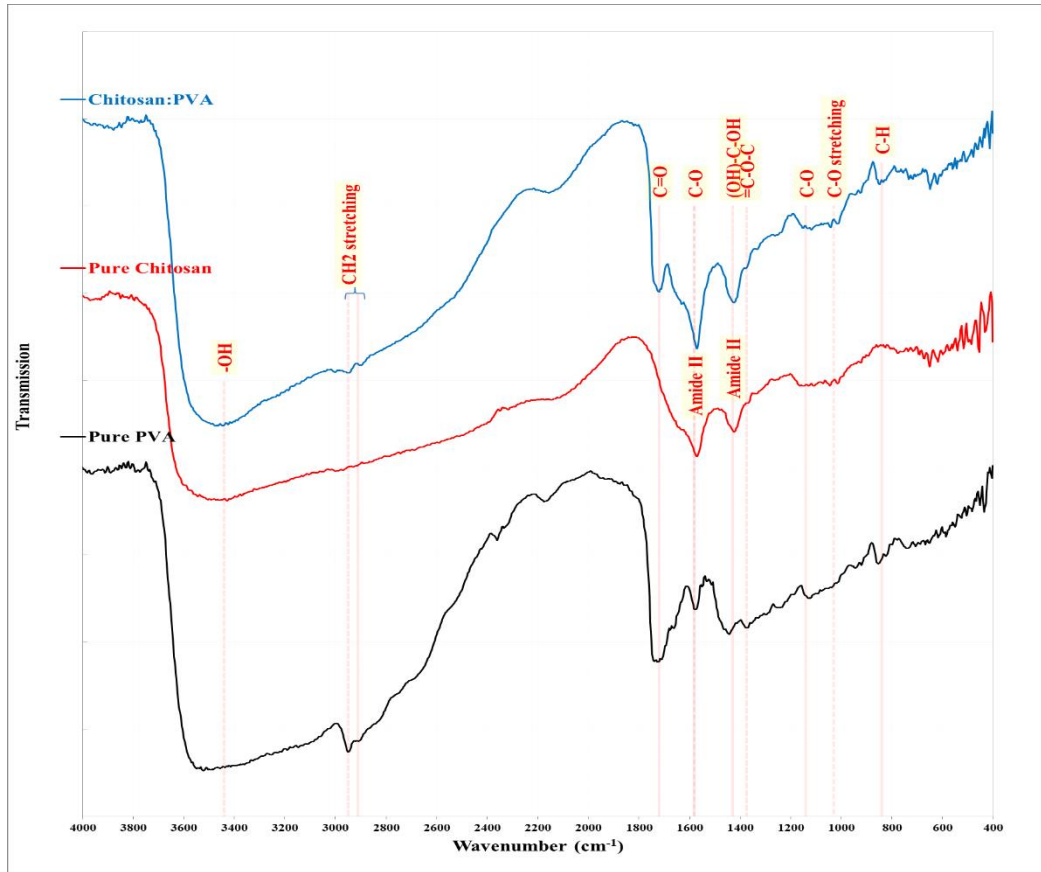


Figure 1: FTIR spectra of pure chitosan, PVA, and chitosan: PVA mixture.

Fig. 2 shows the FTIR spectra of pure Cs: PVA blend and Cs: PVA blend combined with different concentrations of MWCNTs (C1, C2, C3, C4, and C5) [30]. The spectra of CS: PVA blend membrane showed a high-intensity band around 3467.60 cm^{-1} , compared to the spectra of the other samples. This region corresponds to the OH bond involving the interaction of Cs and PVA. In addition, a peak, probably due to the sugar structure, was observed in the range of $3462.89\text{--}3442.29\text{ cm}^{-1}$. The peak at 1725 cm^{-1} is due to the stretching of $\text{C}=\text{O}$ (aromatic) by the aromatic ring system. The band between 3467.60 and 2890 cm^{-1} is related to the stretching vibrations of OH and CH_2 strains. The oscillation observed at 1037.50 cm^{-1} corresponds to the stretching of CO [31]. The FTIR spectrum of the nanocomposites membranes undergoes a peak shift detected by the O-H stretching vibration at 3467.60 cm^{-1} . The C-H vibration is represented at 2950.00 cm^{-1} , the maximum displacement at 1723.75 cm^{-1} is due to $\text{C}=\text{O}$ vibration, and the maximum deviation at 1028 cm^{-1} is due to the observed C-O stretching vibration [14]. The added MWCNTs to the polymer blend created new active groups in the range of $(1627.20, 1633.99, 1633.99, 1630.59, \text{ and } 1630.59)\text{ cm}^{-1}$, as shown in Table 3. This reflects the presence of added MWCNTs dispersed throughout the membrane and caused a decrease in stability and a weakening of the CO bonding strength [32]. The C–O bonds disappeared in the polymer blend but at the same time, the C–O bands appeared, by adding MWCNT [33].

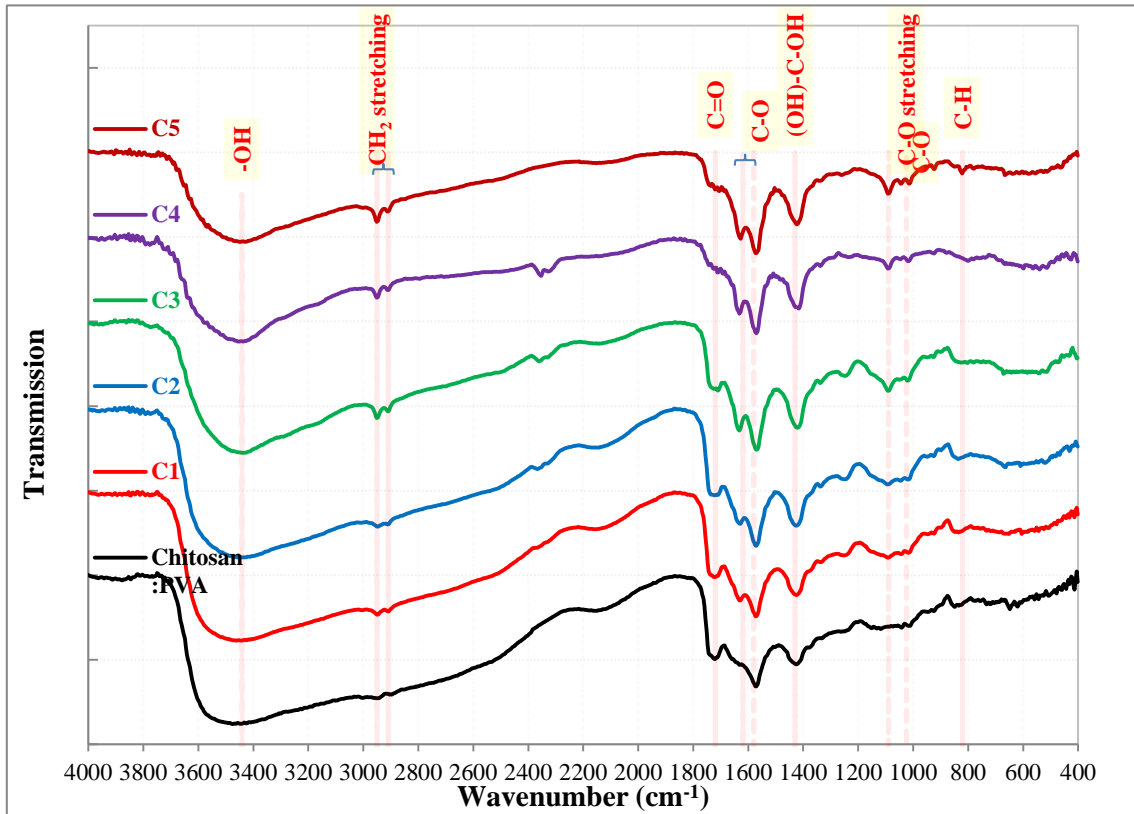


Figure 2: FTIR spectra of chitosan: PVA mixture and nanocomposites incorporated with different percentages of MWCNTs.

Table 2: Bands type and energies for pure chitosan, PVA, and Cs: PVA mixture.

Band Type	Pure PVA	Pure Chitosan	Chitosan: PVA
O-H	3501.25	3482.50	3467.50
CH ₂	2950.00	-	2950.00
C=O	2908.75	-	2901.25
C-O	1727.50	-	1723.75
Amide II	1577.50	-	1570.00
(OH)-C-OH	-	1570.00	-
Amide III	1442.50	-	1423.75
=C-O-C	-	1420.00	-
C-O	1367.50	-	-
C-O stretching	1123.75	1146.25	1123.75
C-O	-	-	1037.50
C-H	853.75	-	842.50

4.2. X-ray Diffraction

Fig. 3 displays the XRD patterns of the pure Cs, PVA, and their mixtures. XRD pattern shows the presence of chitosan amorphous phase [34]. The peaks obtained at $2\theta = 37.2^\circ$, 43.2° , 62.7° , and 75.3° correspond to the (111), (002), (022), and (113) planes of the bulk structure of chitosan, respectively [35]. The characteristic peaks of chitosan at 2θ of 11.9 and 18.6 degrees correspond to the diffraction of (020) and (110) corresponding planes for the orthogonal structure, as reported by Santa et al. [36]. The XRD pattern of PVA shows two strong peaks at $2\theta = 19.6424^\circ$ and 23.2119° belonging to the (101) and (101) planes, respectively, in addition to the weaker plane's crystal peaks, in agreement with Sengwa et al. [37]. The XRD pattern of the Cs: PVA blend exhibits diffraction peaks that were shifted to a lower angle and with a greater magnitude of expansion and decay than the pure PVA sample. These results indicate the formation of Cs: PVA blend by hydrogen bonding [37].

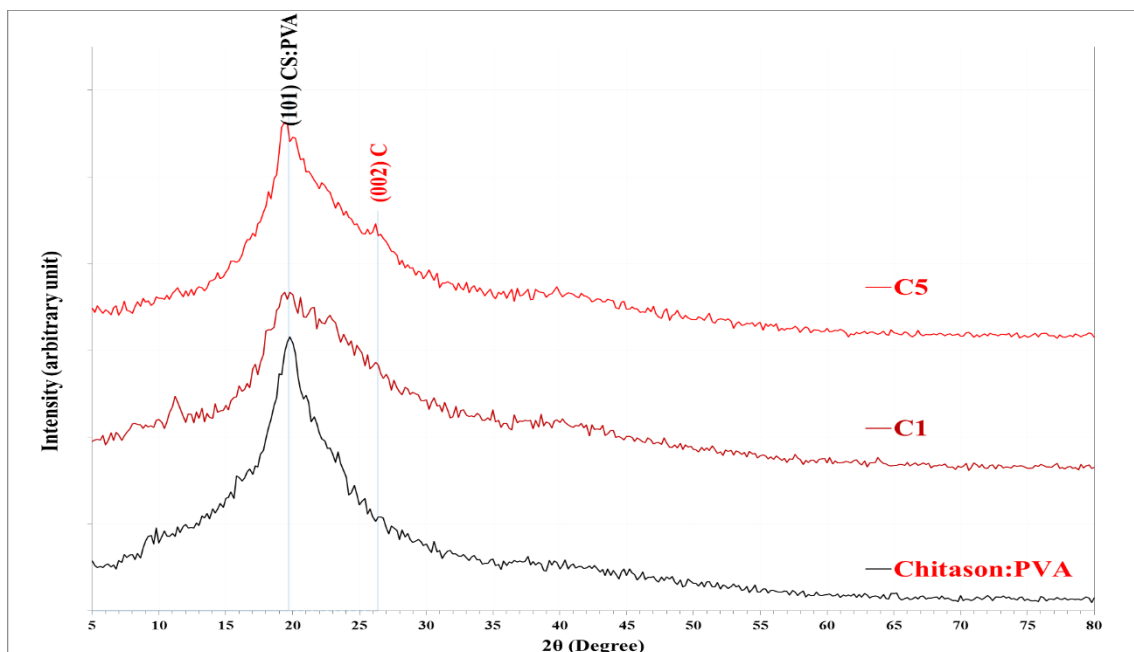


Figure 3: XRD patterns of pure Cs, PVA, and Cs:PVA blend membranes.

Similar observations appeared on the XRD pattern of Cs: PVA filled with different ratios (1, 1.5, 2, 2.5, and 3 wt.%) of MWCNT, as shown in Figure 4. The Cs: PVA blend has similar peaks that were shifted from 19.8609 to 19.7796 , corresponding to hkl (101), after the addition of MWCNTs; also, FWHM decreased with increasing the weight ratio of MWCNTs. A new peak appeared at $2\theta = 26.4706$ corresponding to hkl (002). The FWHM decreased as the percentage of the added MWCNTs increased, as shown in Table 4 [38].

It should be mentioned that the MWCNTs peaks are, to some extent, similar to that of graphite, possibly due to the comparable intrinsic graphene structure featured. CNTs, which are composed of multilayer structures, exhibit similar XRD graphite samples are especially planar (002) [39].

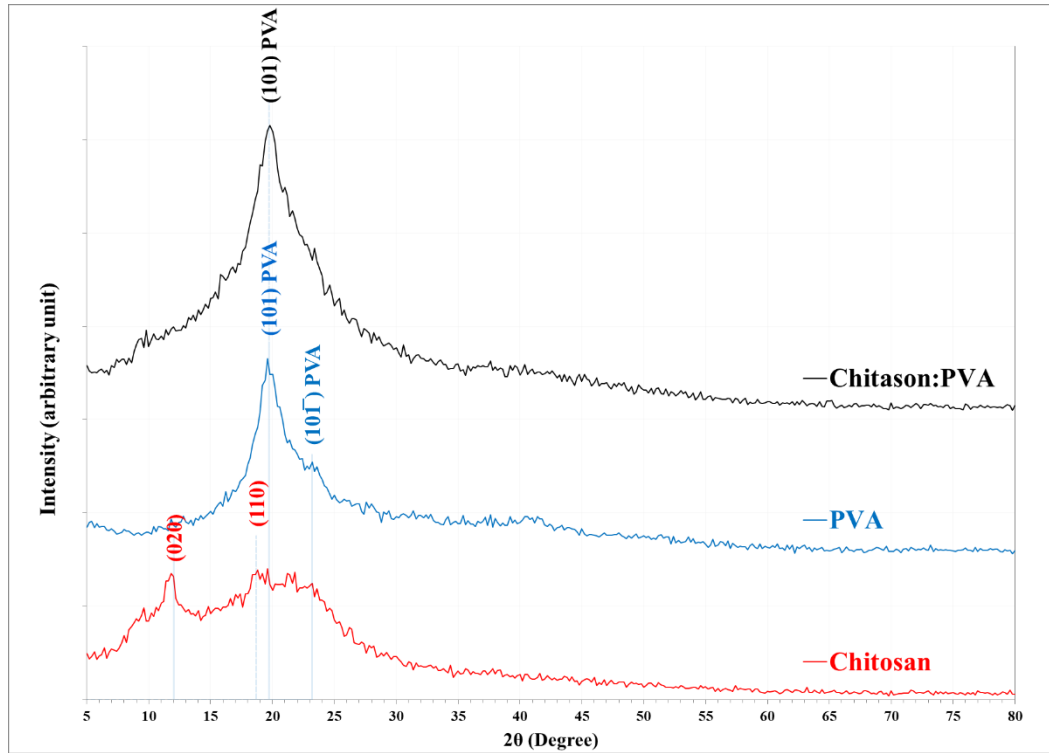


Figure 4: XRD of Cs: PVA blend and blend nanocomposites filled with MWCNT.

Table 4: The calculated crystallinity degree of Cs: PVA blend and MWCNT nanocomposites.

Sample	2θ (Deg.)	FWHM (Deg.)	d_{hkl} (Å)	C.S (nm)	hkl
Chitosan: PVA	19.8609	2.9139	4.4667	2.8	(101)
C1	19.7794	7.9411	4.4850	1.0	(101)
C5	19.5588	5.5147	4.5350	1.5	(101)
	26.4706	1.6177	3.3645	5.0	(002)

4.3. UV–visible Spectroscopy

As light passes through a material, its intensity in the direction of propagation decreases due to absorption and scattering. The loss of energy due to absorption results in the conversion of light energy into other forms of energy, such as lattice oscillations (heat), due to polarized particles in the environment. This excites ions and electrons from the valence band to the conduction band [40]. A valuable method for sample analysis is UV-vis spectroscopy to understand the importance of optical parameters such as band gap energy (E_g) and optical energy absorption of polymer composites in the UV and visible regions. High energy states (σ , π , η orbitals) are described by molecular orbitals [41]. Absorption coefficient, optical band gap, and other optical parameters can easily be determined from UV-vis spectroscopic measurements from 200 to 1100 nm. The UV-vis spectra of the pure blend and those containing MWCNTs are shown in Fig. 5. The samples spectra showed only one absorption peak at about 230 nm. This may be due to the presence of transparency in PVA and Cs. The previously reported data indicate that the $\pi \rightarrow \pi^*$ electronic transition due to unsaturated bonds, mainly determined by C=O bonds, is about 225. As the MWCNTs percentage increases, the resistance also increases. This may be due to the interaction between the

two polymers (Cs: PVA) and the nanomaterial, leading to a slight increase in the wavelength value [11].

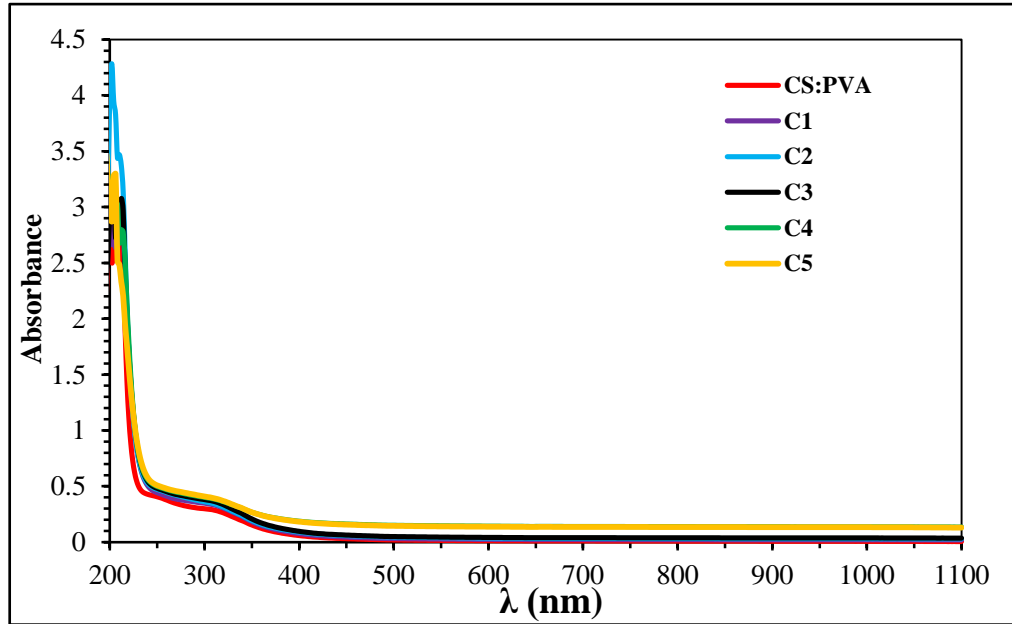


Figure 5: UV-visible spectra of the Cs: PVA polymer blend and the nanocomposites filled with different ratios of MWCNTs.

Optical techniques analyze photochemical transitions and provide data on the bonding structure of organic compounds and the energy gap between crystalline and amorphous samples. Semiconductors are usually divided into two types: (1) Direct deviation, and (2) Indirect deviation. In the direct band gap, the start of the valence band and the rest of the conduction band have the same amplitude of motion [42]. From the optical absorption spectrum, the absorption coefficient (α) can be calculated using the Beer-Lambert relationship (1) as follows:

$$\alpha = 2.303 \frac{A}{L} \quad (1)$$

where: A is the absorbance, α is the absorption coefficient, and L is the film thickness in cm. Analyzing the spectral dependence of absorbance at the absorption edge can determine the optical band gap energy. For example, the present optical data can be analyzed at the near-edge optical absorption according to the following relation:

$$\alpha h\nu = \beta (h\nu - E_g)^r \quad (2)$$

where: E_g is the optical band gap energy, $h\nu$ is the photon incident energy, and (r) is the characteristic phase force in K space. Specifically, (r) takes the values 1, 2, 3, 1/2, and 3/2 Depending on the type of electron transition. The value of (r) is 2 for spatially direct electronic transitions in K space and 1/2 for spatially indirect electronic transitions in indirect energy space. The β coefficient is based on a changing probability and can be considered stable over the optical frequency spectrum. A common method to calculate the value of E_g is plotting $(\alpha h\nu)^2$ versus the absorption edge ($h\nu$) [47], which gives a linear fit over a wide range of $h\nu$, as shown in Fig. 6 [48]. The band gap energy decreased as the MWCNTs percentage increased, as seen in Table 5. The value of the optical band gap energy and the structure band of the material are resolute factors in the implementation and planning of UV-vis [43].

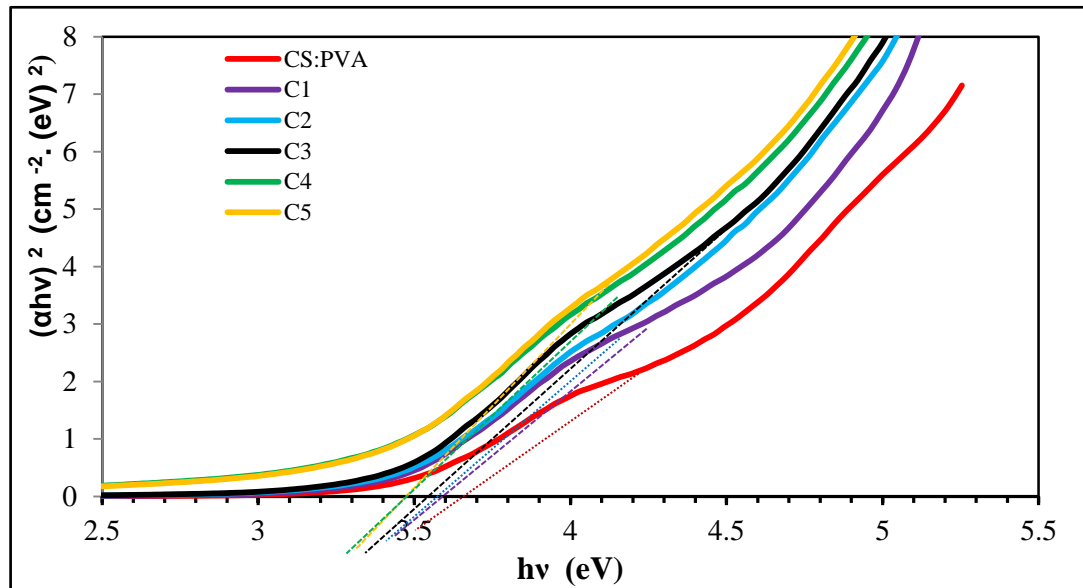


Figure 6: The relation between $(\alpha hv)^2$ vs. photon energy (hv) for Cs: PVA blend, and the blend nanocomposites incorporated with MWCNTs.

Table 5: Band gap energy values.

Sample	E_g (e V)
CS: PVA	3.50
C1	3.45
C2	3.40
C3	3.35
C4	3.30
C5	3.30

4. Conclusions

The following conclusions can be drawn based on the above results: This research synthesized membranes of Cs: PVA blend and the blend nanocomposites filled with MWCNTs using a solution casting procedure. The effects of different concentration ratios of MWCNTs on the optical properties of the film were confirmed. Light transmission for all samples slowed down as the MWCNT concentration increased. From XRD, it was observed that chitosan was composed of irregularly arranged amorphous materials. Then, adding PVA, an ordered texture was observed, and the completely amorphous morphology was transformed into crystalline. The FTIR spectrum shows a chemical interaction between PVA and Cs upon introducing the MWCNTs. Therefore, the CH₂ band can easily be separated from the stretching vibration and made stationary. This study showed that FTIR spectroscopy shows all carboxylic acid and hydroxyl groups in Cs: PVA/MWCNT nanocomposites.

Acknowledgments

The authors would like to thank the University of Baghdad, College of Science, Department of Physics, and the material lab, for assisting us with this article.

Conflict of interest

The authors declare that they have no conflict of interest.

References

1. R. A. Ilyas, H. A. Aisyah, A. H. Nordin, N. Ngadi, M. Y. M. Zuhri, M. R. M. Asyraf, S. M. Sapuan, E. S. Zainudin, S. Sharma, and H. Abral, *Polymers* **14**, 874 (2022).
2. D. J. Hassana and N. A. Ali, *Iraqi J. Phys.* **20**, 26 (2022).
3. Z. B. Roslan, Z. Ramli, M. R. Razman, M. Asyraf, M. Ishak, R. Ilyas, and N. Nurazzi, *Sustainability* **13**, 8705 (2021).
4. S. S. S. Ali, M. R. Razman, A. Awang, M. Asyraf, M. Ishak, R. Ilyas, and R. J. Lawrence, *Sustainability* **13**, 4441 (2021).
5. A. Rozilah, C. A. Jaafar, S. Sapuan, I. Zainol, and R. Ilyas, *Polymers* **12**, 2605 (2020).
6. S. Sapuan, H. Aulia, R. Ilyas, A. Atiqah, T. Dele-Afolabi, M. Nurazzi, A. Supian, and M. Atikah, *Polymers* **12**, 2211 (2020).
7. F. La Mantia and M. Morreale, *Compo. Part A: Appl. Sci. Manuf.* **42**, 579 (2011).
8. R. Ilyas, S. Sapuan, M. Harussani, M. Hakimi, M. Haziq, M. Atikah, M. Asyraf, M. Ishak, M. Razman, and N. Nurazzi, *Polymers* **13**, 1326 (2021).
9. J. Tarique, S. Sapuan, A. Khalina, S. Sherwani, J. Yusuf, and R. Ilyas, *J. Mat. Res. Tech.* **13**, 1191 (2021).
10. A. H. Mohsen and N. A. Ali, *Iraqi J. Sci.* **63**, 4761 (2022).
11. A. Abdelghany, M. Meikhail, A. Oraby, and M. Aboelwafa, *Poly. Bulle.* **80**, 1 (2023).
12. B. T. Iber, N. A. Kasan, D. Torsabo, and J. W. Omuwa, *J. Ren. Mater.* **10**, 1097 (2022).
13. A. Z. Naser, I. Deiab, and B. M. Darras, *RSC Advan.* **11**, 17151 (2021).
14. E. H. Al-Tememe, H. Fatima Malk, and A. Tahseen Alaridhee, *Mater. Today Proce.* **42**, 2441 (2021).
15. N. M. Ali, A. A. Kareem, and A. R. Polu, *J. Inor. Organomet. Poly. Mater.* **32**, 4070 (2022).
16. N. Mulchandani, N. Shah, and T. Mehta, *Poly. Poly. Compos.* **25**, 241 (2017).
17. L. Goettler, K. Lee, and H. Thakkar, *Poly. Rev.* **47**, 291 (2007).
18. S. Parveen, R. Misra, and S. K. Sahoo, *Nanomedicine : nanotechnology, biology, and medicine* **8**, 147 (2012).
19. S. I. Hussein, *Iraqi J. Sci.* **61**, 1298 (2020).
20. J. Chen, S. Wei, and H. Xie, *Journal of Physics: Conference Series* (IOP Publishing, 2021). p. 012184.
21. S. Iijima and T. Ichihashi, *Nature* **363**, 603 (1993).
22. S. Iijima, *Nature* **354**, 56 (1991).
23. M.-F. Yu, O. Lourie, M. J. Dyer, K. Moloni, T. F. Kelly, and R. S. Ruoff, *Science* **287**, 637 (2000).
24. S. L. Shindé and J. Goela, *High Thermal Conductivity Materials* (USA, Springer, 2006).
25. P. Kim, L. Shi, A. Majumdar, and P. L. Mceuen, *Phys. Rev. Lett.* **87**, 215502 (2001).
26. J. Abrahamson, P. G. Wiles, and B. L. Rhoades, *Carbon* **11**, 1873 (1999).
27. S. Tang, P. Zou, H. Xiong, and H. Tang, *Carbohydr. Poly.* **72**, 521 (2008).
28. H. Hu, J. H. Xin, H. Hu, A. Chan, and L. He, *Carbohydr. Poly.* **91**, 305 (2013).
29. S. M. Jasim and N. A. Ali, *Iraqi J. Phys.* **17**, 13 (2019).
30. S. Alamdari, O. Mirzaee, F. N. Jahroodi, M. J. Tafreshi, M. S. Ghamsari, S. S. Shik, M. H. M. Ara, K.-Y. Lee, and H.-H. Park, *Surf. Inter.* **34**, 102349 (2022).
31. E. A. Swady and M. K. Jawad, *AIP Conference Proceedings* (AIP Publishing, 2022). p. 020053.

32. C. Vasile and M. Baican, *Molecules* **26**, 1263 (2021).
33. S. Kumar, B. Krishnakumar, A. J. Sobral, and J. Koh, *Carbohydr. Poly.* **205**, 559 (2019).
34. F. Aljubouri and M. K. Jawad, *Iraqi J. Phys.* **21**, 1 (2023).
35. R. Das, S. Bee Abd Hamid, M. Eaqub Ali, S. Ramakrishna, and W. Yongzhi, *Curr. Nanosci.* **11**, 23 (2015).
36. T. Belin and F. Epron, *Mater. Sci. Eng. B* **119**, 105 (2005).
37. R. Sengwa, S. Choudhary, and P. Dhatarwal, *Advan. Comp. Hyb. Mater.* **2**, 162 (2019).
38. M. I. Shariful, S. B. Sharif, J. J. L. Lee, U. Habiba, B. C. Ang, and M. A. Amalina, *Carbohydr. Poly.* **157**, 57 (2017).
39. M. A. Saleh and M. K. Jawad, *Nano Hyb. Comp.* **35**, 85 (2022).
40. M. A. Pujana, L. Pérez-Álvarez, L. C. C. Iturbe, and I. Katime, *European Poly. J.* **61**, 215 (2014).
41. M. V. D. M. Ribeiro, I. D. S. Melo, F. D. C. D. C. Lopes, and G. C. Moita, *Brazilian J. Pharm. Sci.* **52**, 741 (2016).
42. B. Y. Ahmed and S. O. Rashid, *Arabian J. Chem.* **15**, 104096 (2022).
43. G. Asnag, A. Oraby, and A. Abdelghany, *Comp. Part B: Eng.* **172**, 436 (2019).

تأثير دمج انابيب الكربون متعددة الجدران النانوية على بعض الخصائص الفيزيائية لخليط المتراكبات النانوية

لبنى عبد العزيز جاس¹ ومحمد كاظم جواد¹
تقسم الفيزياء، كلية العلوم، جامعة بغداد، بغداد، العراق

الخلاصة

تم تكوين الاغشية المترابطة المكونة من الشيتوزان (Cs) وبولي فينيل الكحول (PVA) والمتضمن انابيب الكربون متعددة الجدران النانوية للاستفادة من طريقة صب المحلول. تم تحديد الاغشية بالاستفادة من مطياف UV-visible، تحويلات فوريال للاشعة تحت الحمراء (FTIR) وكذلك حيود الاشعة السينية (XRD). استعرضت النتائج ان النماذج مستقرة بشكل كافي وان التفاعلات بين الدقائق النانوية والبوليمرات الغيت بصورة عامة. اظهرت انماط اشعة السينية طور متبلور لبولي فينيل الكحول (PVA) وطور عشوائي للشيتوزان وتبلور أكثر للطور عند ادخال انابيب كربون متعددة الجدران النانوية، وخاصنا عند نسب عالية من MWCNT، الطور المسيطر (002) والذي يرتبط ب الياف الكربون متعددة الجدران النانوية قد تغير الى مرتبة عالية. وصفت مطيافية الاشعة فوق البنفسجية UV-vis المرئية ان النماذج لها قيم امتصاص والتي اشارة بداية حدوث الامتصاص. عند زيادة تركيز الياف الكربون تزداد الشدة وقيم الامتصاص. هذا يكون بسبب مزج Cs ; والمادة النانوية.

الكلمات المفتاحية: Chitosan ، بولي فتيثيل الكحول، أنابيب الكربون النانوية متعددة الجدران، المتراكبات النانوية، الخصائص المورفولوجية.